J|A|C|S ARTICLES

Published on Web 02/10/2009

CdSe/CdS/ZnS Double Shell Nanorods with High Photoluminescence Efficiency and Their Exploitation As Biolabeling Probes

Sasanka Deka,[†,‡] Alessandra Quarta,[†] Maria Grazia Lupo,[‡,§,||] Andrea Falqui,[||] Simona Boninelli,[||] Cinzia Giannini,[⊥] Giovanni Morello,[†] Milena De Giorgi,[†] Guglielmo Lanzani,[§,||] Corrado Spinella,[#] Roberto Cingolani,[†] Teresa Pellegrino,[†] and Liberato Manna*[,†]

National Nanotechnology Laboratory of CNR-INFM, Unità di Ricerca IIT, Distretto Tecnologico ISUFI, via per Arnesano km 5, I-73100 Lecce, Italy, Scuola Superiore ISUFI, University of Salento, Distretto Tecnologico ISUFI, via per Arnesano km 5, I-73100 Lecce, Italy, ULTRAS CNR-INFM, Dipartmento di Fisica, Politecnico di Milano, 20133 Milano, Italy, Fondazione Istituto Italiano di Tecnologia, Via Morego 30 - 16163 Genova, Italy, CNR-Istituto di Cristallografia (IC), via Amendola 122/O, I-70126, Bari, Italy, and CNR-IMM, Sezione di Catania, Stradale Primosole 50, 95121, Catania, Italy

Received October 24, 2008; E-mail: liberato.manna@unile.it

Abstract: We report the synthesis, the structural and optical characterization of CdSe/CdS/ZnS "double shell" nanorods and their exploitation in cell labeling experiments. To synthesize such nanorods, first "dot-in-a-rod" CdSe(dot)/CdS(rod) core/shell nanocrystals were prepared. Then a ZnS shell was grown epitaxially over these CdSe/CdS nanorods, which led to a fluorescence quantum yield of the final core−shell−shell nanorods that could be as high as 75%. The quantum efficiency was correlated with the aspect ratio of the nanorods and with the thickness of the ZnS shell around the starting CdSe/CdS rods, which varied from 1 to 4 monolayers (as supported by a combination of X-ray diffraction, elemental analysis with inductively coupled plasma atomic emission spectroscopy and high resolution transmission electron microscopy analysis). Pump−probe and time-resolved photoluminescence measurements confirmed the reduction of trapping at CdS surface due to the presence of the ZnS shell, which resulted in more efficient photoluminescence. These double shell nanorods have potential applications as fluorescent biological labels, as we found that they are brighter in cell imaging as compared to the starting CdSe/CdS nanorods and to the CdSe/ZnS quantum dots, therefore a lower amount of material is required to label the cells. Concerning their cytotoxicity, according to the MTT assay, the double shell nanorods were less toxic than the starting core/shell nanorods and than the CdSe/ZnS quantum dots, although the latter still exhibited a lower intracellular toxicity than both nanorod samples.

1. Introduction

Within the rapidly advancing research in colloidal nanocrystals of II−VI, III−V, and IV−VI semiconductors for applications in biology and materials science, CdSe is still perhaps the most thoroughly studied nanocrystal system.[1] The emission window of CdSe quantum dots (QDs) can be tuned in the visible spectral range via the control of their diameter. High quality CdSe nanocrystals with narrow size distributions, good crystallinity, and tailored surface properties have now become widely available and have even been commercialized for a few years.[1−4] The fluorescence quantum yield (QY) of the as synthesized nanocrystals is further improved by the growth of a proper epitaxial shell of a higher band gap semiconductor material. Furthermore, such shell growth has been exploited to further tune the range of wavelengths of light emitted from the resulting core−shell nanocrystals, if the band alignments of the core and shell materials are staggered (i.e., type II). In such a case the energy range of emitted photons depends on the relative conduction and valence band offsets for the materials of the core and of the shell.[5−7] Over the past few years core/shell QDs have been widely investigated as fluorescent biomarkers,

[†] National Nanotechnology Laboratory of CNR-INFM.
[‡] University of Salento.
[§] ULTRAS CNR-INFM.
[||] Fondazione Istituto Italiano di Tecnologia.
[⊥] CNR-Istituto di Cristallografia.
[#] CNR-IMM.

(1) Rosenthal, S. J.; McBride, J.; Pennycook, S. J.; Feldman, L. C. *Surf. Sci. Reports* **2007**, *62* (4), 111–157.
(2) Murray, C. B.; Norris, D. J.; Bawendi, M. G. *J. Am. Chem. Soc.* **1993**, *115*, 8706–8715.
(3) Peng, Z. A.; Peng, X. G. *J. Am. Chem. Soc.* **2001**, *123* (1), 183–184.
(4) Qu, L. H.; Peng, Z. A.; Peng, X. G. *Nano Lett.* **2001**, *1* (6), 333–337.
(5) Peng, X. G.; Schlamp, M. C.; Kadavanich, A. V.; Alivisatos, A. P. *J. Am. Chem. Soc.* **1997**, *119* (30), 7019–7029.
(6) Dabbousi, B. O.; RodriguezViejo, J.; Mikulec, F. V.; Heine, J. R.; Mattoussi, H.; Ober, R.; Jensen, K. F.; Bawendi, M. G. *J. Phys. Chem. B* **1997**, *101* (46), 9463–9475.
(7) Hines, M. A.; Guyot-Sionnest, P. *J. Phys. Chem.* **1996**, *100* (2), 468–471.

 10.1021/ja808369e CCC: $40.75

due to their photochemical stability and high brightness, which makes them a good alternative to organic fluorophores.[8−10]

For CdSe, depending on the specific application requirements, different semiconductor materials have been exploited for the shell growth, such as for instance CdS,[5,11,12] ZnS,[6,7,13,14] ZnSe,[14,15] and ZnTe.[16,17] Recently CdSe/CdS/ZnS or CdSe/ZnSe/ZnS "double shell" QDs have been reported,[18,19] where the outer ZnS shell serves as potential barrier to confine the charge carriers inside the CdSe/CdS or the CdSe/ZnSe regions. In such systems CdS or ZnSe is first deposited on the CdSe to partially accommodate the strain and reduce the formation of defects in the shell. These double-shell nanocrystals have been investigated for what concerns their optical properties and their potential biological applications. In the case of nanorods (NRs), much fewer examples of core/shell systems have been developed so far. In 2002 Manna et al. reported the growth of a CdS/ZnS graded shell on CdSe NRs which however could only reach fluorescence QYs around 20−30%,[20] while in 2003 Talapin et al. developed the growth of an asymmetric, rod-like CdS shell over roughly spherical CdSe QDs, which led to highly emissive, "dot-in-a-rod" core−shell NRs.[21] Recently, Carbone et al. and Talapin et al. have independently published a high temperature seeded growth of CdSe/CdS core/shell NRs, again based on a "dot-in-a-rod" structure, with easily controllable aspect ratio and again high fluorescence QY.[22,23]

In principle, there are several unique optical properties that can make NRs potentially more appealing bioimaging probes than QDs.[22−30] Semiconductor NRs, in addition to the tunable range of wavelengths of the emitted light (mainly achieved by variation of the NR diameter) and which makes them similar to QDs, exhibit linearly polarized emission, such as in the case of CdSe NRs and CdSe/CdS "dot-in-a-rod" nanocrystals.[22,24] Additionally, NRs exhibit a larger Stokes shift,[24] faster radiative decay[27] and slower bleaching kinetics than QDs. Recently, Alivisatos's and Prasad's groups have demonstrated independently for instance that CdSe/CdS/ZnS NRs (CdSe NR core and CdS/ZnS graded shell) can be used efficiently as optical probes to target cancer cells and for single molecule fluorescence imaging.[28,29] Yong et al. have shown that the same type of NRs conjugated to targeting molecules such as transferrin or folic acid can be used as an efficient optical tracking probes for multiplex labeling of cancer cells in vitro.[30] Despite all these favorable properties and first encouraging results of NRs, the main issue with semiconductor nanocrystals as fluorescent labels, especially those containing Cd, remains still their compatibility with living systems, which limits their potential impact as diagnostic tools, and even for in vitro studies. To fully exploit the potential advantages of semiconductor NRs in biological applications, there is therefore the need to develop nanocrystals that are as bright and as stable as possible, so that at least for in vitro studies their cytotoxicity is reduced as less material would be required to label cells.

We report here the growth of a ZnS shell around "dot-in-a-rod" CdSe/CdS NRs, which raises further the photochemical stability and fluorescence QY of the starting CdSe/CdS nanocrystals in solution and furthermore reduces the toxic effects of NRs on cells. Detailed X-ray diffraction, elemental analysis with inductively coupled plasma atomic emission spectrometry and high resolution transmission electron microscopy analysis revealed the formation of 1−4 monolayers of wurtzite ZnS shell around the CdSe/CdS NRs. The passivation of surface traps led to QY values up to 75% for the double shell NRs, which represents an increase of about 25% with respect to the starting CdSe/CdS NRs. Subpicosecond carrier dynamics, measured by the pump−probe technique, revealed that the additional ZnS shell increases the average number of photogenerated charge carriers that are not trapped and therefore relax into the CdSe core, where radiative recombination occurs, whereas time-resolved PL spectroscopy confirms the reduced defect density in double shell NRs. The measurements also indicate that the charge transfer mechanism at the CdS/CdSe interface and the electron wave function delocalization into the CdS shell are not affected by the presence of the ZnS shell.

These double shell NRs, along with their parent CdSe/CdS NRs and with standard CdSe/ZnS QDs, were properly surface-functionalized in order for them to be stable in a biological environment and were compared with each other as biological labels for cells. The cytotoxicity results of administrating these three samples to HeLa (human carcinoma) cells showed that the double shell NRs are less toxic compared to the starting core/shell NRs and also to CdSe/ZnS QDs (although the latter still exhibited a lower intracellular toxicity than the two NR samples). Furthermore, due to the higher QY of the double shell NRs reported here with respect to CdSe/CdS NRs and especially

(8) Kirchner, C.; Liedl, T.; Kudera, S.; Pellegrino, T.; Javier, A. M.; Gaub, H. E.; Stolzle, S.; Fertig, N.; Parak, W. J. *Nano Lett.* **2005**, *5* (2), 331–338.
(9) Lee, J.; Kim, J.; Park, E.; Jo, S.; Song, R. *Phys. Chem. Chem. Phys.* **2008**, *10* (13), 1739–1742.
(10) Mattoussi, H.; Mauro, J. M.; Goldman, E. R.; Anderson, G. P.; Sundar, V. C.; Mikulec, F. V.; Bawendi, M. G. *J. Am. Chem. Soc.* **2000**, *122* (49), 12142–12150.
(11) Schlamp, M. C.; Peng, X. G.; Alivisatos, A. P. *J. Appl. Phys.* **1997**, *82* (11), 5837–5842.
(12) Li, J. J.; Wang, Y. A.; Guo, W. Z.; Keay, J. C.; Mishima, T. D.; Johnson, M. B.; Peng, X. G. *J. Am. Chem. Soc.* **2003**, *125* (41), 12567–12575.
(13) Steckel, J. S.; Zimmer, J. P.; Coe-Sullivan, S.; Stott, N. E.; Bulovic, V.; Bawendi, M. G. *Angew. Chem., Int. Ed.* **2004**, *43* (16), 2154–2158.
(14) Huang, G. W.; Chen, C. Y.; Wu, K. C.; Ahmed, M. O.; Chou, P. T. *J. Cryst. Growth* **2004**, *265* (1−2), 250–259.
(15) Reiss, P.; Bleuse, J.; Pron, A. *Nano Lett.* **2002**, *2* (7), 781–784.
(16) Kim, S.; Fisher, B.; Eisler, H. J.; Bawendi, M. *J. Am. Chem. Soc.* **2003**, *125* (38), 11466–11467.
(17) Chen, C. Y.; Cheng, C. T.; Yu, J. K.; Pu, S. C.; Cheng, Y. M.; Chou, P. T.; Chou, Y. H.; Chiu, H. T. *J. Phys. Chem. B* **2004**, *108* (30), 10687–10691.
(18) Talapin, D. V.; Mekis, I.; Gotzinger, S.; Kornowski, A.; Benson, O.; Weller, H. *J. Phys. Chem. B* **2004**, *108* (49), 18826–18831.
(19) Lim, S. J.; Chon, B.; Joo, T.; Shin, S. K. *J. Phys. Chem. C* **2008**, *112* (6), 1744–1747.
(20) Manna, L.; Scher, E. C.; Li, L. S.; Alivisatos, A. P. *J. Am. Chem. Soc.* **2002**, *124* (24), 7136–7145.
(21) Talapin, D. V.; Koeppe, R.; Gotzinger, S.; Kornowski, A.; Lupton, J. M.; Rogach, A. L.; Benson, O.; Feldmann, J.; Weller, H. *Nano Lett.* **2003**, *3* (12), 1677–1681.
(22) Carbone, L. *Nano Lett.* **2007**, *7* (10), 2942–2950.
(23) Talapin, D. V.; Nelson, J. H.; Shevchenko, E. V.; Aloni, S.; Sadtler, B.; Alivisatos, A. P. *Nano Lett.* **2007**, *7* (10), 2951–2959.
(24) Hu, J. T.; Li, L. S.; Yang, W. D.; Manna, L.; Wang, L. W.; Alivisatos, A. P. *Science* **2001**, *292* (5524), 2060–2063.
(25) Htoon, H.; Hollingworth, J. A.; Malko, A. V.; Dickerson, R.; Klimov, V. I. *Appl. Phys. Lett.* **2003**, *82* (26), 4776–4778.
(26) Rothenberg, E.; Kazes, M.; Shaviv, E.; Banin, U. *Nano Lett.* **2005**, *5* (8), 1581–1586.
(27) Shabaev, A.; Efros, A. L. *Nano Lett.* **2004**, *4* (10), 1821–1825.
(28) Fu, A. H.; Gu, W. W.; Boussert, B.; Koski, K.; Gerion, D.; Manna, L.; Le Gros, M.; Larabell, C. A.; Alivisatos, A. P. *Nano Lett.* **2007**, *7* (1), 179–182.
(29) Yong, K. T.; Qian, J.; Roy, I.; Lee, H. H.; Bergey, E. J.; Tramposch, K. M.; He, S. L.; Swihart, M. T.; Maitra, A.; Prasad, P. N. *Nano Lett.* **2007**, *7* (3), 761–765.
(30) Yong, K. T.; Roy, I.; Pudavar, H. E.; Bergey, E. J.; Tramposch, K. M.; Swihart, M. T.; Prasad, P. N. *Adv. Mater.* **2008**, *20* (8), 1412–1417.

with respect to the CdSe/ZnS QDs, less amount of material is required for cell labeling.

2. Experimental Section

2.1. Chemicals. Cadmium oxide (CdO, 99.5%), hexadecylamine (HDA, 98%), diethylzinc (Et_2Zn,1.0 M solution in hexane) and hexamethyldisilathiane ($(TMS)_2S$) were purchased from Sigma-Aldrich. Trioctylphosphine oxide (TOPO 99%), trioctylphosphine (TOP, 97%), tributylphosphine, (TBP, 97%), sulfur (99%), selenium (Se, 99,99%) and dimethyl cadmium (Me_2Cd, 97% 10 weight% in hexane) were purchased from Strem Chemicals. Octadecylphosphonic acid (ODPA, 99%) and hexylphosphonic acid (HPA, 99%) were purchased from Polycarbon Industries. Poly(maleic anhydride-alt-1-tetradecene) was purchased from Sigma-Aldrich, although at present this polymer is not available commercially any more (readers can however refer to a new polymer coating procedure that employs a similar polymer, which is commercially available (ref 31). Sodium tetraborate decahydrate, boric acid, *N*-(3-dimethylaminopropyl)-*N*′-ethylcarbodiimide hydrochloride (EDC), tris-borate-EDTA buffer, 3-(4,5-dimethyl-2-thiazolyl)-2,5-diphenyl-2H-tetrazolium bromide (MTT salt), as well as all the disposable materials and the products needed for cell culture were purchased from Sigma-Aldrich. Diamine-PEG 897 was purchased from Fluka. Agarose (D-1 low EEO) was purchased from Eppendorf.

2.2. Synthesis of Spherical CdSe Nanocrystals and CdSe/CdS NRs. Following a procedure published by our group, spherical CdSe nanocrystals were synthesized in a TOPO-ODPA mixture of surfactants at 370−380 °C and were used as seeds to synthesize CdSe/CdS core/shell NRs in a TOPO-ODPA-HPA mixture at 350 °C.[22] Detailed synthesis procedures of the CdSe nanocrystals and CdSe/CdS core/shell NRs are reported in the Supporting Information. After the synthesis, the core/shell NRs were precipitated from the reaction mixture by using methanol and were redispersed in 1 mL of toluene or chloroform for further use.

2.3. Synthesis of CdSe/CdS/ZnS NRs. (A) Stock Solution for ZnS Shell Growth. For the synthesis of double shell NRs, two different stock solutions were prepared. For the growth of a "ZnS-only" shell, stock solutions for Zn and S precursors were prepared by dissolving 0.630 g of Et_2Zn and 0.152 g of $(TMS)_2S$ in 4.1 g of TBP. For a graded shell of CdS/ZnS the stock solution was prepared as described in the literature[20] with a modification of the Cd concentration: 0.5 g of Et_2Zn solution and 37 mg of the Me_2Cd solution were mixed in TBP and to this solution 76 mg of $(TMS)_2S$ were added. The resulting solution was then diluted with 2.05 g of TBP. The molar ratios of Zn:Cd:S in the final stock solution were 1.00:0.012:0.63.

(B) Procedure for Shell Growth onto CdSe/CdS NRs. Either 4 g of TOPO or a mixture of 3 g of TOPO and 1.5 g of HDA was first degassed in a 50 mL three-neck flask at 120 °C for 1 h, after which 0.5 mL of the CdSe/CdS solution in toluene were added. The flask was then pumped to vacuum for 30 min in order to remove the toluene. The concentration of the starting NRs inside the reaction flask was approximately equal to 1.45×10^{-9} M. To overcoat CdSe/CdS NRs with the second shell, after pumping to vacuum the reaction mixture was heated to 160−180 °C under N_2. For the epitaxial growth of the ZnS shell or of the CdS/ZnS graded shell, the Zn/S or Zn/Cd/S precursors solution was injected dropwise. The typical injection rate was 0.1 mL/min and the amount of injected solution was around 0.5−1.0 mL, depending on the desired thickness of the shell. Aliquots of the growth solution were taken from time to time and their absorption and fluorescence spectra were recorded to check the progress in the shell growth. After the injection, the solution was cooled to 100 °C (within 30 min) and was kept at that temperature for another 10 min. Upon cooling to room temperature, 5 mL of anhydrous butanol were added to the reaction mixture and the final solution was stored under air. Methanol was added to precipitate the NRs from this solution. After centrifugation, the precipitate was dissolved either in toluene, if various characterizations had to be carried out on it, or in chloroform if the sample had to undergo a polymer coating to be used for cell studies.

2.4. Surface Functionalization of Nanocrystals. CdSe/CdS/ZnS NRs, CdSe/CdS NRs, and additionally a sample of spherical CdSe/ZnS QDs (the latter synthesized following a method described in the literature,[6] see Supporting Information) were transferred into aqueous environment by means of a polymer coating procedure.[32] The polymer molecules form a uniform and stable shell around the nanoparticles, which now display outstretched carboxy groups. Diamino-PEG molecules (NH_2-PEG-NH_2, molecular weight 897 Da) were then bound to these polymer-coated nanocrystals through the formation of an amide bond between the carboxy group of one polymer molecule and one of the two amino groups of the PEG (see Supporting Information for further details).

2.5. Transmission Electron Microscopy (TEM). Samples for TEM were prepared by dropping dilute solutions of nanocrystals onto carbon coated copper grids and letting the solvent evaporate. TEM images were recorded on a JEOL Jem 1011 microscope operating at 100 kV. Phase-contrast high-resolution TEM (HRTEM) measurements were performed with a Jeol 2100F microscope, equipped with a field emission gun and working at the accelerating voltage of 200 kV. The Energy Filtered TEM (EFTEM) analyses were carried out on a 200 kV energy filtered transmission electron microscope JEOL JEM 2010F with a Gatan image filter (GIF).

2.6. Elemental Analysis. Elemental analysis was carried out via Inductively Coupled Plasma Atomic Emission Spectroscopy (ICP-AES), using a Varian Vista AX spectrometer. Samples were dissolved either in concentrated HNO_3 solutions or in concentrated HCl/HNO_3 3:1 (v/v).

2.7. UV−Vis Absorption, Photoluminescence (PL) Spectroscopy, and Determination of PL QY. Absorption measurements were carried out using a Varian Cary 300 UV−vis spectrophotometer. PL spectra were recorded on a Varian Cary Eclipse fluorescence spectrophotometer with an intense Xenon flash lamp. The gradient method was adopted to estimate the photoluminescence QY of the various samples,[33] using Rhodamine G6 as reference fluorescent dye, and by exciting all the samples at 488 nm. Briefly, ethanol solutions at different concentrations of Rhodamine 6G were prepared, and their absorption and fluorescence spectra were recorded (using a 10 mm optical path fluorescence cuvette). The concentration range of these solutions was such that their optical densities at their excitation wavelength (488 nm), were between 0.01 and 0.1, to avoid self-absorption effects[34] in the photoluminescence spectra. The optical densities (at 488 nm) and the integrated fluorescence intensities of the various samples were then reported in a graph (optical densities in abscissas and integrated PL intensities in ordinates). The series of points was then interpolated with a straight line of slope m_{Dye} and which in principle should have intercept equal to zero. The same approach was adopted for each nanocrystal sample (CdSe/CdS core shell NRs, CdSe/CdS/ZnS double shell NRs and CdSe/ZnS QDs), that is, for each of them different solutions of NCs (in toluene or water) at various concentrations were prepared, and their absorption and integrated PL were plotted and fitted with a straight line, yielding therefore for each type of nanocrystal an interpolation line of slope m_{NC} and intercept close to zero. The PL QY from each nanocrystal sample was then calculated using the following equation:

(31) Di Corato, R.; Quarta, A.; Piacenza, P.; Ragusa, A.; Figuerola, A.; Buonsanti, R.; Cingolani, R.; Manna, L.; Pellegrino, T. *J. Mater. Chem.* **2008**, *18* (17), 1991–1996.

(32) Pellegrino, T.; Manna, L.; Kudera, S.; Koktysh, D.; Rogach, A.; Keller, S.; Radler, J.; Natile, G.; Parak, W. J. *Nano Lett.* **2004**, *4*, 703–707.

(33) Lakowicz, J. R. *Principles of Fluorescence Spectroscopy*; Plenum: New York, 1983.

(34) Dhami, S.; De Mello, A. J.; Rumbles, G.; Bishop, S. M.; Phillips, D.; Beeby, A. *Photochem. Photobiol.* **1995**, *61*, 341.

$$QY_{NC} = QY_{Dye} \frac{m_{NC}}{m_{Dye}} \cdot \left(\frac{\eta_{solvent}}{\eta_{ethanol}} \right)^2$$

where QY_{Dye} is the QY of Rhodamine G6 (which is known from the vendor) and $\eta_{ethanol}$ and $\eta_{solvent}$ are the refractive indexes of the solvents in which the dye and the nanocrystal sample are dissolved, respectively. More details and plots are provided in the Supporting Information section.

2.8. Time-Resolved Spectroscopy. Ultrafast carrier dynamics was investigated by using a standard pump−probe setup, based on a chirp amplified Titanium-sapphire laser system,[35,36] with 150 fs time resolution. All measurements were performed on solutions of core/shell or double shell NRs dispersed in toluene at room temperature, at magic angle between pump and probe polarization, to exclude transient anisotropy effects onto dynamics.[36,37] The used pump energy was 3.2 eV (390 nm), and in the two series of measurements that were carried out the pump fluences for all samples were 40 μJ/cm^2 and 265 μJ/cm^2, respectively. Time-resolved photoluminescence spectroscopy measurements were performed at low temperature (10 K) by exciting the nanorods with the second harmonic (405 nm) of a Ti:sapphire laser (80 fs pulses at 80 MHz repetition rate). The signal was collected by a spectrograph (0.35 m focal length) and detected by a streak camera, with a resulting temporal resolution of 12 ps. The measurements were performed by varying the excitation density from 0.03 to 100 μJ /cm^2 per pulse.

2.9. Powder X-Ray Diffraction (XRD). XRD measurements were performed with a Rigaku-Inel diffractometer equipped with a 12 kW ceramic tube with a copper anode, a Ge(111) single crystal monochromator and a CPS120 INEL detector. Concentrated nanocrystal solutions were spread on top of a silicon miscut substrate, after which the sample was allowed to dry and was then measured in reflection geometry. Data were collected at a fixed incident angle of about 1°.

2.10. Gel Electrophoresis. PEG functionalized nanocrystals were characterized by gel electrophoresis. Electrophoretic runs were carried out through a 2% agarose gel at 100 V for 1 h on a Biorad system. Prior to gel electrophoresis, to each sample a solution corresponding to 20% of the sample volume and containing Orange G and 30% glycerol in loading buffer was added. After the run, the gel was observed under UV light.

2.11. Dynamic Light Scattering. (DLS) measurements were performed on PEG functionalized nanocrystals using a Zetasizer Nano ZS90 (Malvern) equipped with a 4.0 mW He−Ne laser, operating at 633 nm, and an avalanche photodiode detector. All the samples were filtered through 0.2 μm filters before analysis. The average hydrodynamic diameter of the PEG conjugated and of the polymer coated nanocrystals was evaluated.

2.12. Cell Culture and Cell Viability Assay. HeLa (human carcinoma) cells were grown at 37 °C and under 5% CO_2 atmosphere in RPMI-1640 medium, supplemented with L-glutamine (2 mM), penicillin (100 units/mL), streptomycin (100 μg/mL), and 10% heat-inactivated fetal bovine serum (PBS). A viability assay (MTT test) was performed using the 3-(4,5-dimethyl-2-thiazolyl)-2,5-diphenyl-2H-tetrazolium bromide on HeLa cells added with CdSe/CdS and CdSe/CdS/ZnS NRs and CdSe/ZnS QDs. In detail, 5×10^4 cells suspended in 1 mL of medium were seeded in each well of a 12 well-plate, and after 24 h incubation at 37 °C, the medium was replaced with a fresh medium (1 mL into each well) containing the nanocrystals at various total Cd concentrations (5, 50, 500 μM, as found by elemental analysis, see section 2.7). After additional 24 h of incubation at 37 °C, the medium was removed, the cells were washed twice with phosphate buffer (pH 7.4), and 1 mL of fresh medium serum-free containing 1 mg/mL of MTT was added into each well. After 3 h of incubation at 37 °C, the MTT, reduced by the mitochondrial reductase of vital cells, formed a dark insoluble product, the formazan. From each well the medium was collected, centrifuged, and then discarded. The dark pellet was dissolved in 2 mL of DMSO, leading to a violet solution whose absorbance at 570 nm was determined. The absorbance can be correlated to the percentage of vital cells, by comparing the data of the doped cells with those of the control cells (with no nanocrystals added).

2.13. Determination of the Intracellular Cd Concentration. To estimate the intracellular Cd concentration ($[Cd]_{cell}$) and consequently the degree of intracellular uptake of nanocrystals, 10^5 cells suspended in 2 mL of medium were seeded in each well of a 6 well-plate. After 24 h incubation at 37 °C the medium was replaced with 2 mL of fresh medium per each well containing the nanocrystals at a total Cd concentration equal to 50 μM. After again 24 h of incubation at 37 °C, the medium was removed, the cells were washed twice with phosphate buffer (pH 7.4), they were trypsinized and counted using a cell-counting chamber. In detail, 500 μL of trypsin were added into each well and, after 5 min incubation at 37 °C, the cell suspension was collected and 1.5 mL of PBS was added in order to recover any remaining cells from each well. The suspension was transferred into a cuvette, the PL spectra were recorded and the PL intensities were normalized to the number of cells. For the determination of the intracellular Cd uptake, the cell suspensions were digested by adding 2 mL of a HCl/HNO_3 3:1 (v/v) solution (as reported in the previous paragraph) and the intracellular Cd concentration was measured by means of elemental analysis. The intracellular Cd concentration was converted into intracellular nanoparticle concentration by a method described in the Supporting Information.

2.14. Confocal Microscopy Imaging. Confocal microscopy images of HeLa cells that had uptaken the nanocrystals were recorded on an Olympus FV-1000-microscope equipped with an argon laser source (excitation 488 nm) with a DM488/405-type dicroic filter and acquisition window at 615 ± 20 nm.

3. Results and Discussion

3.1. Epitaxial Growth of the ZnS Shell. In preliminary attempts to grow the ZnS shell on CdSe/CdS NRs, only Zn/S precursors were employed in various surfactants (i.e., TOPO or mixtures of TOPO and HDA). In these experiments, we did not observe the formation of a ZnS shell but rather the separate nucleation of small ZnS nanocrystals, and the final QY of the resulting NRs was even lower than that of the starting NRs. A considerable increase in QY was observed on the other hand when the solution of Zn/Cd/S shell precursors was employed for the shell growth, similarly to what was found by Manna et al. for a graded shell growth on CdSe NRs.[20] It appeared therefore that the addition of minute amounts of cadmium in the Zn/S precursor solution (which were actually ten times lower here than the amount of Cd used by Manna et al.[20]) helped the formation of a shell. It is likely that in analogy with the previous report of Manna et al., also this shell had somehow a graded composition, that is, it was more enriched in Cd at the monolayer(s) in direct contact with the CdS substrate than on the outer part of the shell, which should be composed almost exclusively of ZnS. In the current work the minute amounts of Cd precursors act as a "binder", that is, they initiate the growth of the ZnS shell, which otherwise does not appear to take place.

3.2. Characterization of the Double Shell NRs. The TEM and HRTEM images of the starting core/shell NRs and of the corresponding double shell NRs are shown in Figure 2. In all samples the distribution of NR lengths and diameters is relatively narrow. The size of the starting CdSe/CdS NRs (as shown in

(35) Polli, D.; Luer, L.; Cerullo, G. *Rev. Sci. Instrum.* **2007**, *78* (10), 103108.
(36) Gadermaier, C.; Lanzani, G. *J. Phys.: Condens. Matter* **2002**, *14* (42), 9785–9802.
(37) Malkmus, S.; Kudera, S.; Manna, L.; Parak, W. J.; Braun, M. *J. Phys. Chem. B* **2006**, *110* (35), 17334–17338.

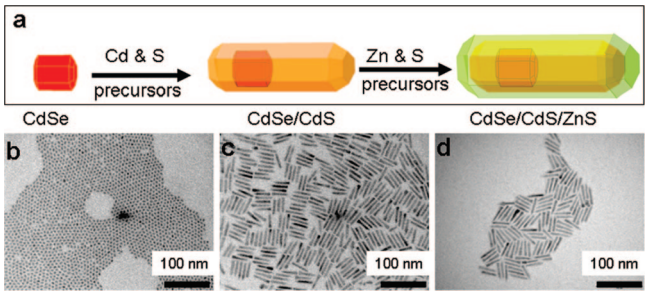

Figure 1. (a) Sketch describing the growth of CdS NRs over CdSe cores, and the growth of a ZnS shell over the resulting CdSe/CdS NRs to form double shell CdSe/CdS/ZnS NRs. TEM image of (b) starting CdSe cores, (c) CdSe/CdS NRs, and (d) CdSe/CdS/ZnS NRs, the latter grown in TOPO.

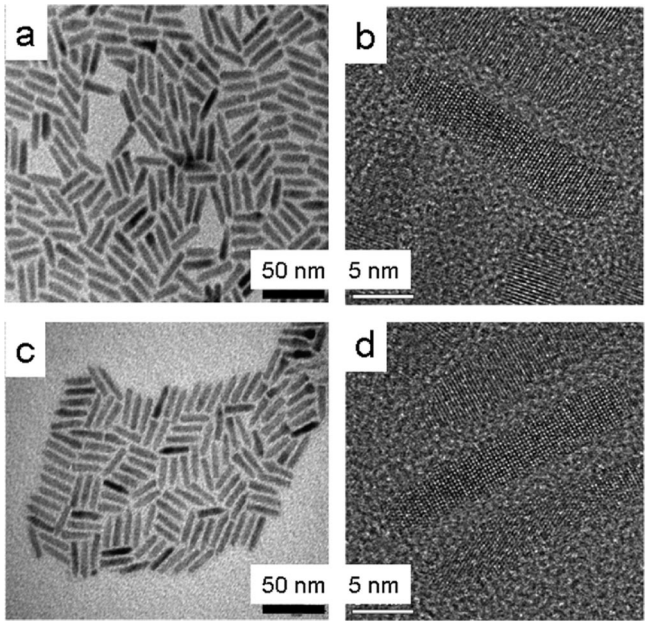

Figure 2. TEM images of starting CdSe/CdS NRs (a) and of the corresponding CdSe/CdS/ZnS double shell NRs grown in a TOPO/HDA mixture (c). The corresponding HRTEM images of representative NRs for each sample are shown in the right side panels (b and d).

Figure 2a) is 5 (diameter) × 24 nm (length). Via a statistical analysis of a large number of nanorods from TEM and HRTEM images we could appreciate a small increase in these dimensions in the corresponding double shell sample (Figure 2c). The increase in diameter is ∼1 nm, whereas the increase in length is ∼2 nm. This corresponds to a growth of roughly 1.0−2.0 monolayers of CdS/ZnS shell over the lateral sides of the NRs, whereas around 3.0−4.0 monolayers grow at the rod tips, that is, along the *c* axis. This is consistent with the higher reactivity and lower interfacial strain of the {001} and {00$\bar{1}$} facets of wurtzite nanocrystals, as documented extensively in the literature.[21,38] The final average dimension of the double shell NRs shown in Figure 2c was 6 × 26 nm. The crystallinity of CdSe/CdS core/shell and CdSe/CdS/ZnS double shell samples can be assessed from the HRTEM images (b, d) of Figure 2. Fourier analysis of HRTEM images indicates that preferential growth along CdS ⟨002⟩ direction occurred, and shows no noticeable evidence of differences in the measured lattice

(38) Peng, Z. A.; Peng, X. G. *J. Am. Chem. Soc.* **2001**, *123* (7), 1389–1395.

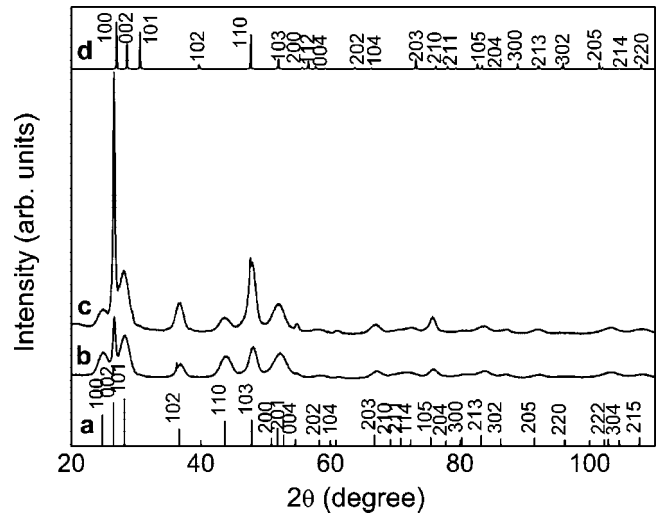

Figure 3. Powder X-ray diffraction patterns of CdSe/CdS core/shell NRs (b) and CdSe/CdS/ZnS double shell NRs (c). The bulk XRD patterns of wurtzite CdS (a) and ZnS (d) are also shown.

spacings between the core and the outer part as well as at the tip of CdSe/CdS/ZnS NRs, implying epitaxial growth of the second shell, as expected in the case of growth of few ZnS monolayers on the CdSe/CdS NR (i.e., the difference in lattice parameters between CdS and ZnS could not be appreciated by our TEM setup, especially for the present case of only a few monolayers of ZnS material). Unfortunately, energy filtered analyses were not of much help in discriminating the presence of the ZnS, although by them we could locate the presence of the CdSe seeds inside single rods (see Supporting Information).

The powder X-ray diffraction patterns of the starting CdSe/CdS core/shell NRs and of the corresponding CdSe/CdS/ZnS double shell NRs are shown in Figure 3. The 2θ positions of XRD reflections in the core/shell as well as in the double shell NRs match with the reflections from the CdS wurtzite crystalline phase (the contribution to diffraction from the CdSe core is negligible as well as that from the ZnS shell). No shift in the peak position is measured between the two samples in the whole angular range (20−110 deg), indicating that the ZnS shell does not induce any additional strain on the original core/shell NRs. The only detected effect which can be ascribed to the ZnS extra shell is a slight reduction of the 002 peak width. Indeed the full width at half-maximum (fwhm) of the 002 peak shrinks from 0.427 deg, measured on the CdSe/CdS core/shell NRs, to 0.314 deg on the CdSe/CdS/ZnS double shell NRs. The shrinking in the peak width can be explained by a bigger domain of the double shell sample along the 002 direction with respect to the core/shell sample. This suggests a preferential growth of the ZnS shell along the 002 direction, mainly at the rod tips, but also an epitaxial regime of the growth at the CdS/ZnS heterointerface, as also supported by their slight increase in length observed by TEM and HRTEM analyses.

Elemental analysis carried out on both the core/shell and the double shell samples indicated the presence of Zn in the latter samples. The amounts of Zn obtained from the ICP measurement are given in Table 1. On the basis of the Cd and Zn concentration estimated from elemental analysis, the XRD analysis, and the average sizes determined by TEM/HRTEM analyses, we have estimated the numbers of monolayers of CdS/ZnS graded shell. These are shown in Table 1.

3.3. Optical Properties. The formation of the ZnS shell could be further assessed by monitoring the optical absorption spectra.

Table 1. NR Dimensions, Zn Concentration from ICP, and Number of ZnS Monolayers

sample	NR diameter (nm)	NR length (nm)	Zn concentration (from ICP) ($\times 10^{-3}$M)	number of shell monolayers: lateral direction	number of shell monolayers: longitudinal direction
CdSe/CdS NRs	5.0 ± 0.5	24.0 ± 2	0	0	0
CdSe/CdS/ZnS NRs	6.0 ± 0.5	26.0 ± 2	8.41	1.6	3.2

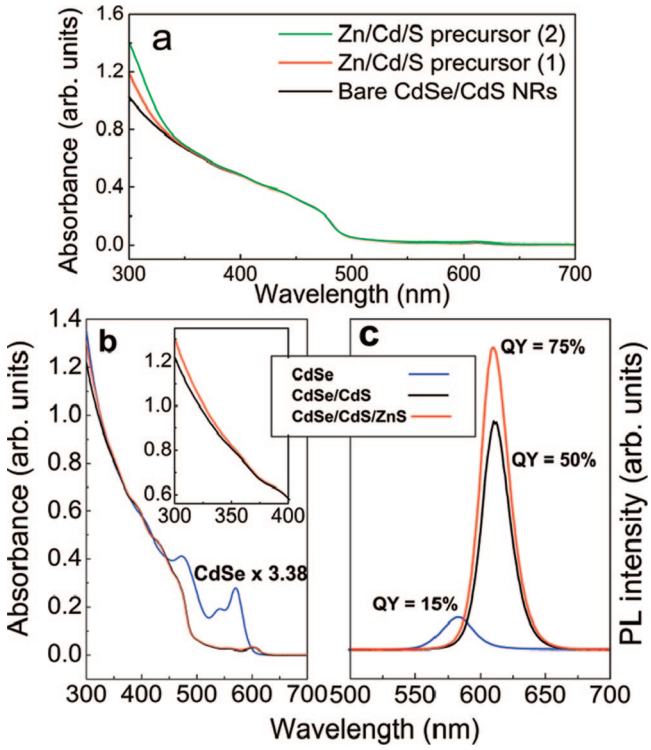

Figure 4. (a) Absorption spectra of aliquots taken during the addition of Cd/Zn/S precursors to a solution of CdSe/CdS NRs. (b-c) Comparison of absorption, PL and QY of the starting CdSe nanocrystals of the CdSe/CdS core/shell NRs and finally of the double shell CdSe/CdS/ZnS NRs, for a representative sequence of experiments of double shell growth. The average diameter of the CdSe core used in this study was 3.5 nm, the diameter vs length of the core/shell rod and double shell rod was 5.0 nm × 24.0 and 6.0 nm × 26.0 nm, respectively. (b) Observed red shift of the absorption spectra of CdSe/CdS NRs with respect to the CdSe cores shows that the CdS shell cannot provide potential barriers that are large enough to prevent the leakage of the exciton into the shell, mainly due to electron leakage.[22] On the other hand, no shifts in peak position are observed neither in absorption nor in PL when a ZnS shell is grown on these CdSe/CdS NRs. Only a (tiny) shoulder appears in the absorption spectra (see inset in b) due to the growth of a ZnS shell. The effect of the ZnS shell growth is more evident in the PL spectra. Furthermore, in the present case, further additions of shell precursors for the ZnS growth resulted in an actual decrease of the PL QY.

These are shown in Figure 4a for the starting core/shell NRs and of the corresponding double shell NRs with increasing shell thickness. For CdSe/CdS NRs, a dominating absorption edge at around 483 nm is evident, corroborating the energy band gap of nanosized CdS (2.56 eV).[22,23] The other noticeable change in the spectra is the evolution of a broad absorption below 360 nm with the addition of Zn/Cd/S precursor, which can be ascribed to the formation of the ZnS shell.[39,40] Dabbousi et al. already described this type of shoulder in the ultraviolet region

Table 2. Relevant Parameters Involved in the Determination of the Photoluminescence QYs for the Various Samples

sample	m^a	R^{2b}	QY (%)[c]	solvent[d]
Rhodamine G6	2.50×10^5	0.999	95	ethanol
CdSe/CdS NRs	1.1×10^5	1	50	toluene
CdSe/CdS/ZnS NRs	1.63×10^5	0.998	75	toluene
CdSe/ZnS QDs	3.96×10^4	0.997	18	toluene
Rhodamine 6G	1.45×10^5	0.995	95	ethanol
CdSe/CdS NRs (polymer coated)	6.00×10^4	1	38	water
CdSe/CdS/ZnS NRs (polymer coated)	6.93×10^4	0.999	44	water
CdSe/ZnS QDs (polymer coated)	1.31×10^4	0.997	8	water

[a] Slope (m) of the fitted curve. [b] Goodness-of-fit (R^2). [c] Quantum efficiencies of the different samples and of the dye. [d] Solvents used. Refractive indexes of solvents at 20 °C:[45] ethanol = 1.3611, toluene = 1.4961, water = 1.333. The second sets of measurements (with polymer coated samples) were carried out in the conventional PMMA cuvettes used for biological/aqueous samples.

with increasing ZnS coverage as a result of direct absorption into the higher band gap ZnS shell.[6] The intensity of this absorption increases by increasing the amount of Zn/Cd/S precursor added. The same behavior has been observed for double shell nanorods synthesized using TOPO as solvent. It is also worth pointing out that such a shoulder in the absorption spectra remained even after the nanocrystals were precipitated from the growth solution (by addition of small amounts of methanol) and the precipitate was redissolved in toluene. This indicates that the shoulder was not due to the separate nucleation of small ZnS nanocrystals but indeed was due to the growth of a ZnS shell.

The absorption, photoluminescence and QY of the starting spherical CdSe nanocrystals, of the corresponding CdSe/CdS NRs and of the final CdSe/CdS/ZnS NRs are compared in Figure 4b and c. Different plots of QY measurements are discussed in the Supporting Information and the measured QYs of different samples are reported in Table 2. The average diameter of the starting CdSe nanocrystals used as seeds to grow the CdSe/CdS NRs, was ~3.5 nm, and the PL QY was around 15%. The formation of a thick, rod-like CdS shell around the CdSe cores resulted in a large increase in PL QY up to about 50%, which was accompanied by a red shift of both the first optical absorption peak and PL band (Figure 4a and b). The growth of an outer ZnS shell around the CdSe/CdS nanocrystals did not result however in any red shift, neither in the absorption nor in the PL spectra. Also, the PL peak remained symmetric and sharp. The PL QY of CdSe/CdS/ZnS NRs could be as high as 75%. This proves a better passivation of the surface states of CdS by the wide band gap ZnS shell. However, such increases in QY could be appreciated only if small amounts of shell precursors were added (i.e., 0.5−1.0 mL), therefore, only if a very thin shell was grown. Further additions caused instead a decrease in PL QY. We performed control experiments in which the CdSe/CdS NRs were dissolved either in TOPO or in a TOPO/HDA mixture and heated at the same temperatures used for the growth of the second shell, but no shell precursors were added. In these experiments, we noted a decrease in the PL QY, indicating that the increase in the PL QY upon addition of the shell precursors was the result of a shell growth, rather than of a surfactant exchange process.

(39) Lu, S. Y.; Wu, M. L.; Chen, H. L. *J. Appl. Phys.* **2003**, *93* (9), 5789–5793.

(40) Li, Y. C.; Li, X. H.; Yang, C. H.; Li, Y. F. *J. Phys. Chem. B* **2004**, *108* (41), 16002–16011.

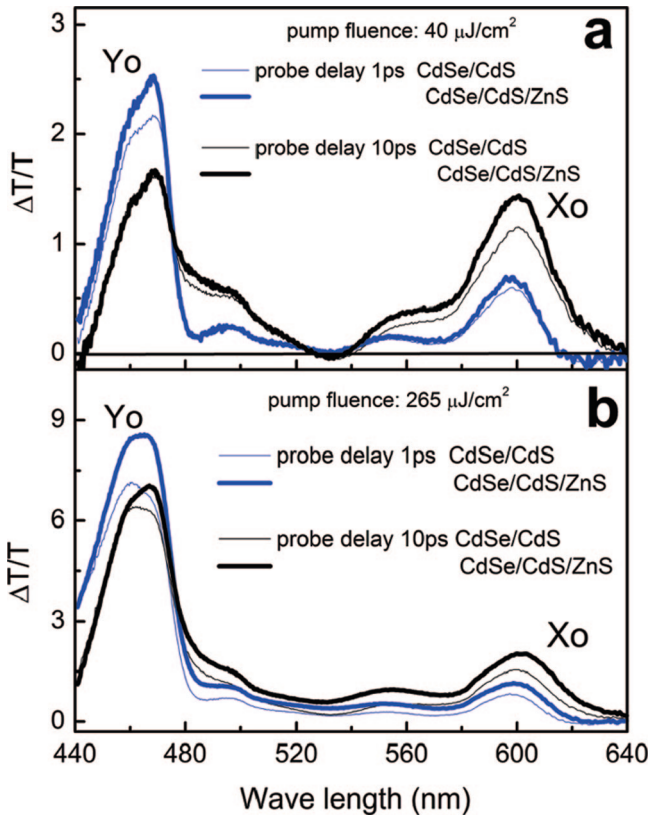

Figure 5. Differential transmission spectra at pump fluences equal to 40 μJ/cm^2 (a) and 265 μJ/cm^2 (b) for CdSe/CdS NRs (thin line) and for CdSe/CdS/ZnS NRs, (thick line). The spectra were taken at probe delays of 1 ps (blue line) and 10 ps (black line). The bleaching peak labeled as Yo and Xo correspond to the lowest lying energy levels in CdS and CdSe, respectively.

3.4. Time-Resolved Spectroscopy Results. The chirp free differential transmission (ΔT /T) spectra for two representative samples of CdSe/CdS core/shell and CdSe/CdS/ZnS double shell NRs, respectively, at different pump and probe delays and at two different pump fluences are shown in Figure 5. The pump excitation mainly reached CdS transitions, placing carriers in the inner shell. The two peaks labeled as Xo and Yo correspond to bleaching of the band edge transition in the CdSe dot and in CdS regions of the samples, respectively. The reported spectra show that, at a fixed pump excitation, the bleaching at Yo is stronger (has a larger amplitude) in the double shell CdSe/CdS/ZnS NR sample than in the CdSe/CdS core/shell NR sample, giving evidence that in the double shell NR sample there is a greater amount of charge relaxing at the lower lying levels of the CdS shell. After 1 ps Xo is still rising while Yo is decaying: the maximum value at Xo, well evident at a probe delay of 10 ps, is larger in the double shell NR sample. The slow rise of Xo is assigned to rod-dot hole transfer.[41] These ΔT /T spectra have been normalized to sample concentration (to do so, each spectrum was normalized at the amplitude of Xo in the linear absorption spectrum) to allow for comparison of absolute signals. In this way, the differences in state filling between the single and the double shell NR samples can be inferred from the amplitude of the ΔT /T bleaching.

In Figure 6, the normalized bleaching kinetics at Xo and Yo for core/shell and double shell samples, at pump fluence of 40 μJ/cm^2 and of 265 μJ/cm^2, are reported. The inset in Figure 6a shows the initial stage of the bleaching kinetics at Xo and Yo and gives evidence that the time rise at Xo corresponds to the initial stage of bleaching decay at Yo for both samples. Higher bleaching at Xo for the double shell NR sample in the spectra in Figure 5 suggests that a larger fraction of the nascent carrier population reaches the CdSe dot region. This result is further confirmed by comparison of the time evolution of the bleaching kinetics at Yo (Figure 6). At a fixed pump excitation, the bleaching at Yo decays faster in the double shell sample than in the single shell one. This points to a lower degree of carrier trapping in the double shell sample, which leads to higher density of free carriers in the nanocrystal and hence to a faster decay of Y_O due to an increased rate of Auger recombination.[42]

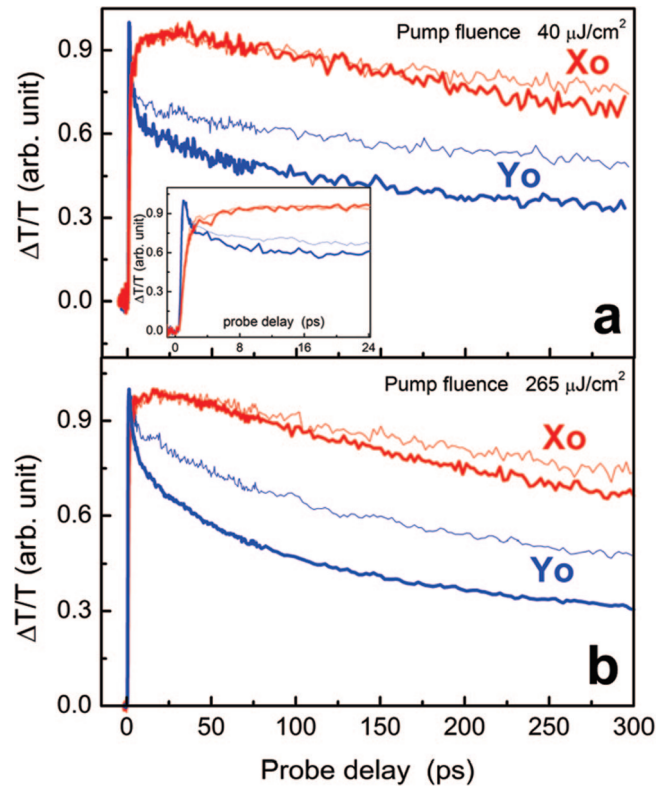

Figure 6. Differential bleaching kinetics at the different pump excitations of 40 μJ/cm^2 (a) and 265 μJ/cm^2 (b), for double shell CdSe/CdS/ZnS NRs (thick line) and for core/shell CdSe/CdS NRs (thin line) reported for Yo (blue line) and Xo (red line). The inset in (a) shows the initial stage of the bleaching kinetics at Xo and Yo.

Figure 7 reports the PL decay of the core/shell and double shell NR samples as measured at low temperature (10 K). Both curves are well fitted by a biexponential function. The lifetimes are comparable in the two samples within the experimental error. We found $t_1 = 335 \pm 14$ ps, $t_2 = 3.0 \pm 0.1$ ns for the core/shell NR sample, and $t_1 = 322 \pm 13$ ps, $t_2 = 2.9 \pm 0.1$ ns for the double shell NR sample. The difference relies on the relative contribution of the faster component on the whole decay. It accounts for 49% and 40% in the core/shell and in the double shell NR samples, respectively. Interestingly this contribution, along with the lifetime, remains constant over a broad range of excitation densities (0.03/100 μJ/cm^2), demonstrating that it is not due to Auger recombination mechanisms. We attribute the slow component to the intrinsic radiative decay time, whereas the shortest component is related to fast carrier decay from

(41) Lupo, M. G.; Della Sala, F.; Carbone, L.; Rossi, M. Z.; Fiore, A.; Luër, L.; Polli, D.; Cingolani, R.; Manna, L.; Lanzani, G. *Nano Lett.* **2008**, *8* (12), 4582–4587.

(42) Klimov, V. I. *J. Phys. Chem. B* **2000**, *104* (26), 6112–6123.

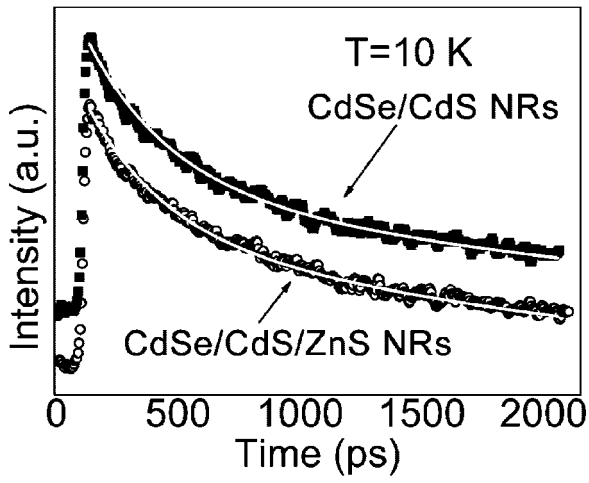

Figure 7. PL decay of core/shell (filled symbols) and double shell (empty symbols) NRs recorded at low temperature (10 K) and at an excitation density of 60 μJ/cm^2, and relative biexponential best fit curves (white lines).

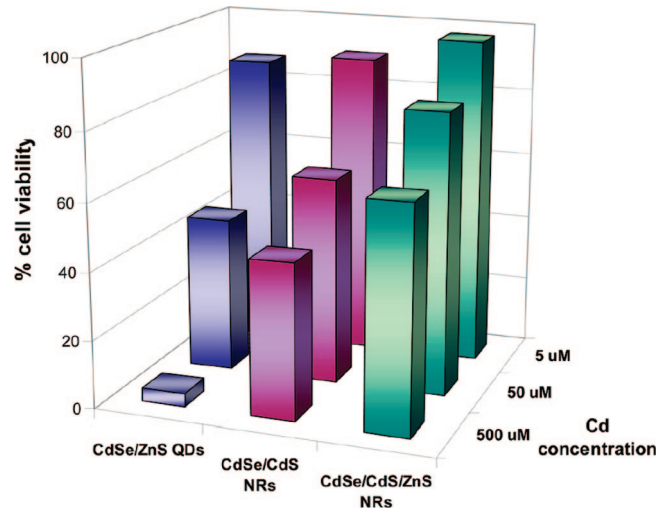

Figure 8. Cell viability assay of CdSe/ZnS QDs, CdSe/CdS NRs, and CdSe/CdS/ZnS NRs performed on HeLa cells (all nanocrystal samples were polymer coated and further functionalized with PEG molecules). For each nanocrystal sample, three different $[Cd]_{sol}$ were administered to cells, namely 5, 50, and 500 μM.

intrinsic states to defect states, 330 ps being the time occurring for carrier trapping. Therefore, the different relative contributions reinforce the hypothesis of a lower density of trap states in the double shell sample with respect to the core/shell NR sample, as inferred both by the different QYs between the two samples and by the pump−probe data.

In conclusion, both pump−probe and time-resolved photoluminescence measurements reported here confirm that the presence of the ZnS shell reduces the presence of trap states at the CdS surface, and consequently leads to an increased probability for charge carrier decay at CdSe emitting states, and therefore to an increased quantum efficiency.

3.5. Preparation and Characterization of Water Soluble Nanocrystals. The detailed water solubilization and characterization of the CdSe/ZnS QDs, CdSe/CdS NRs and CdSe/CdS/ZnS NRs are reported in the Supporting Information (see Figure S6 and S7, Supporting Information). For all samples, the transfer in water and their further functionalization with PEG led to a decrease in their PL QY, as reported in Table 2, in agreement with other reports.[43,44] In water, the PL QY of the double shell NRs was slightly higher than that of the starting CdSe/CdS NRs (see Table 2).

3.6. Cell Studies. The main target of this study was to evaluate the cytotoxic effect of the nanocrystals along with their fluorescent labeling features, as all the samples used in this study contained Cd. In the various samples that were synthesized the average number of Cd atoms per nanocrystal was obviously different, because of differences in shape, size and composition among the samples. Therefore, when comparing the effects of different types of nanocrystals on cells, the concentrations of nanocrystals in the various solutions that were administered to the cells were adjusted such that all solutions contained the same total concentration of Cd ($[Cd]_{sol}$), as determined by elemental analysis. In the cell viability assay three series of experiments were performed in which PEG-coated nanocrystals (CdSe/ZnS QDs, CdSe/CdS NRs, and CdSe/CdS/ZnS NRs) were administered to HeLa cells and incubated for 24 h at 37 °C. In each series, solutions were prepared at the same $[Cd]_{sol}$ (namely 5, 50, and 500 μM). The results of the MTT viability test are reported in Figure 8. As expected, for all nanocrystal samples, higher $[Cd]_{sol}$ administered led to an increased toxic effect on the cells. For a given $[Cd]_{sol}$ administered to the cell medium, the experiments on cells treated with double shell NRs displayed a percentage of cell viability that was higher than that of the cells treated either with the CdSe/CdS core−shell NR sample or with the CdSe/ZnS QD sample. This effect was more pronounced at $[Cd]_{sol}$ = 500 μM, for which the cell viability was around 65% for the double shell NR sample, less than 50% for the CdSe/CdS core/shell NR sample and below 10% for the CdSe/ZnS QD sample. In general, a reduced cytotoxicity of the double shell sample was observed and could be estimated as being around 20% lower than that of its parent CdSe/CdS core/shell NR sample.

To shed light on the apparent lower toxicity of the double shell NRs with respect to their parent CdSe/CdS NRs and also to the CdSe/ZnS QDs, a more careful analysis had to be carried out and for this we needed to estimate the intracellular Cd concentration ($[Cd]_{cell}$). To this aim, for each of the three nanocrystals samples, a nanocrystal solution at $[Cd]_{sol}$= 50 μM was administered to the cells. We caution the reader that in terms of concentration of nanocrystals ($[Nanocrystal]_{sol}$) that of NRs in the two NR samples was significantly lower than that of QDs, since each NR (whether core/shell or double shell) contained on average many more Cd atoms than each CdSe/ZnS QD (see Table 3, column 3). After 24 h of incubation time the medium was removed, the cells were counted and the Cd amount up-taken by the cells was measured, which yielded the average intracellular Cd concentration $[Cd]_{cell}$ (see Table 3, column 4). Approximately the same intracellular Cd concentration $[Cd]_{cell}$ was found in cells doped either with core/shell NRs or with double shell NRs, while a slightly lower concentration was found in cells doped with the QD sample. Such differences however are not very significant given the substantial errors associated with these estimates. A similar trend was observed when the same series of experiments were carried out on two other cell lineages, namely KB and MCF7 cells (data not

(43) Smith, A. M.; Duan, H. W.; Rhyner, M. N.; Ruan, G.; Nie, S. M. *Phys. Chem. Chem. Phys.* **2006**, *8* (33), 3895–3903.
(44) Breus, V. V.; Heyes, C. D.; Nienhaus, G. U. *J. Phys. Chem. C* **2007**, *111* (50), 18589–18594.
(45) Lide, D. R. *CRC Handbook of Chemistry and Physics*, 81st ed.; CRC Press: Boca Raton, FL, 2001.

Table 3. Relevant Parameters Involved in the Measurement of Intracellular Cd and Nanocrystal Concentrations in HeLa Cells (100 000 Cells) Incubated with CdSe/ZnS QDs, CdSe/CdS core/shell NRs, and Double Shell CdSe/CdS/ZnS NRs for 24 h

Sample	$[Cd]_{sol}$ ($\times 10^{-5}$ M)[a]	$[Nanocrystal]_{sol}$ ($\times 10^{-8}$ M)[b]	$[Cd]_{cell}$ ($\times 10^{-7}$ M)[c]	$[Nanocrystal]_{cell}$ ($\times 10^{-10}$ M)[d]	$[Nanocrystal]_{cell}/[Nanocrystal]_{sol}$ ($\times 10^{-2}$ M)[e]
CdSe/ZnS QDs (PEG coated)	5.0	4.3	4.7 ± 1.3	4.20	0.97
CdSe/CdS NRs (PEG coated)	5.0	0.56	6.6 ± 2.8	0.79	1.4
CdSe/CdS/ZnS NRs (PEG coated)	5.0	0.56	6.0 ± 1.7	0.78	1.39

[a] Total concentration of Cd in each solution of nanocrystals administered to the cells ($[Cd]_{sol}$). [b] Concentration of nanoparticles in each solution ($[Nanocrystal]_{sol}$). For the two NR samples (the core/shell NR and the double shell NR sample) the same Cd concentration corresponded in practice to the same concentration of nanocrystals. [c] Intracellular Cd concentration ($[Cd]_{cell}$). Each of the values displayed in this column is the average of three independent experiments performed on HeLa cells and is referred to the intracellular Cd concentration estimated on 10^5 cells. [d] Intracellular concentration of nanoparticles ($[Nanocrystal]_{cell}$). [e] Ratio of intracellular nanocrystal concentration, as reported in column 4, to the total nanoparticle concentration in the starting solutions, as reported in column 2 (i.e., $[Nanocrystal]_{cell}/[Nanocrystal]_{sol}$). The data indicate that there is no much difference among the various nanocrystal samples in the degree of nanoparticle uptake by the cells.

Table 4. Relevant Parameters Involved in the Evaluation of the Cytotoxicity of the Various Nanocrystal Samples

sample	number of nanoparticles uptaken by each cell $NP = [Nanocrystal]_{cell}$ ($2 \times 10^{-3} \cdot 6.022 \times 10^{23} \cdot 10^{-5}$)[a]	total surface per unit volume of nanoparticles per cell $\xi = (A/V) \cdot NP$ (nm^{-1})[b]	% killed cells[c]	(% killed cells $\cdot 10^{-2}$) $\cdot$ $10^5/\xi$ (cells $\cdot$ nm)[d]
CdSe/ZnS QDs (PEG coated)	5.1×10^6	5.5×10^6	54	1.0×10^{-2}
CdSe/CdS NRs (PEG coated)	9.5×10^5	1.0×10^6	39	3.9×10^{-2}
CdSe/CdS/ZnS NRs (PEG coated)	9.4×10^5	1.0×10^6	17	1.7×10^{-2}

[a] Number of nanoparticles uptaken by each cell, calculated over 10^5 cells. [b] Estimate of the total surface area per unit of volume of nanoparticles that is exposed to the intracellular environment for the three samples studied (i.e., the parameter ξ). A/V corresponds to the surface area/volume ratio of a single nanoparticle. [c] Percentage of killed cells, as determined by the MTT viability test for the three samples studied. [d] Normalized "ξ-related intracellular toxicity" of the various nanocrystal samples, calculated as ratio of the killed cells (column 4) over the parameter ξ (column 3).

shown). In terms of intracellular concentration of nanocrystals ($[Nanocrystal]_{cell}$), that of NRs (Table 3, column 6) was again lower than that of the QDs. Based on these results the first remark that can be made is that the nanoparticle toxicity is rather related to the intracellular concentration of nanocrystals $[Nanocrystal]_{cell}$ than to $[Cd]_{cell}$. Another important remark is that the ratio of nanoparticles up-taken by the cells to the total number of particles in the solutions to which the cells had been exposed ($[Nanocrystal]_{cell}/[Nanocrystal]_{sol}$ ratio) is not much different in the various experiments, and suggests that there is no striking difference in the degree of nanoparticle uptake by the cells between NRs and QDs, at least in the cases studied in the present work.

To embed in a single parameter the intracellular concentration of the three nanocrystal samples under investigation and their geometrical features (i.e., shape and size), and to correlate such parameter to the toxicity of nanocrystals on cells, we determined for each sample the "total surface per unit volume" of nanocrystals exposed to the intracellular environment. Under the assumption that the shape of QDs is roughly a sphere and that of NRs is roughly a cylinder, we calculated the area (A) and the volume (V) of each type of nanoparticle (using data from TEM). The A/V ratio was then multiplied by the intracellular number of nanoparticles, that is, the average number of nanoparticles uptaken by each cell to yield a parameter (which we name as "ξ") that can be correlated to the "total surface per unit volume" of nanoparticles exposed per cell. This parameter ξ is reported in Table 4, column 2, for the various samples. QDs exhibited the highest value of surface per unit volume ξ exposed to the intracellular medium,[46−50] and therefore the higher toxicity of the QDs with respect to the two NR samples is related to their higher total surface per unit volume exposed to the intracellular environment.

The comparison above however does not shed any light on how the toxicity of nanocrystals is related to their type of surface, which is unique for each of the three nanocrystal samples under investigation. A better comparison in this respect among the samples can be made for instance by normalizing the number of killed cells to the above "total surface per unit volume" ξ parameter. This yields a new parameter (reported in Table 4, column 3) which we call "normalized ξ-related intracellular toxicity" of each of the three types of nanocrystal samples, or in other words their toxicity (number of killed cells) if their intracellular "total surface per unit volume" were the same (and actually equal to one) in all the experiments.

The data of Table 4, column 5, show that the intracellular toxicities (as defined above) of the various nanocrystals are all of the same order of magnitude, and actually the QDs appear as being less toxic than both NR samples. The lower intracellular toxicity of the surface of QDs with respect to that of the two NR samples should be due to their uniform coverage with the ZnS shell, which significantly reduces leakage of Cd atoms in the cell,[46,48] while this leakage should be substantial in the core/shell NRs samples, as the CdS surface is separated by the intracellular environment only by its organic coating layer. We also found a lower intracellular toxicity for double shell NRs (which exhibited actually the highest MTT viability) with respect to the core/shell NRs, as again the ZnS shell in CdSe/CdS/ZnS NRs should help to reduce the Cd release. As the various structural analyses have indicated, the ZnS shell growth occurs mainly at the tips of the NRs (i.e., the aspect ratio of the double shell NRs was slightly larger than their parent CdSe/CdS NRs), and therefore we can deduce that the tips of the NR are the main sources of release of Cd to the environment. This is

(46) Derfus, A. M.; Chan, W. C. W.; Bhatia, S. N. *Nano Lett.* **2004**, *4* (1), 11–18.
(47) Chan, W. H.; Shiao, N. H.; Lu, P. Z. *Toxicol. Lett.* **2006**, *167*, 191–200.
(48) Lovric, J.; Cho, S. J.; Winnik, F. M.; Maysinger, D. *Chem. Biol.* **2005**, *12* (11), 1227–1234.
(49) Zhang, Y. B.; Chen, W.; Zhang, J.; Liu, J.; Chen, G. P.; Pope, C. *J. Nanosci. Nanotechnol.* **2007**, *7* (2), 497–503.
(50) Liu, Y. F.; Chen, W.; Joly, A. G.; Wang, Y. Q.; Pope, C.; Zhang, Y. B.; Bovin, J. O.; Sherwood, P. *J. Phys. Chem. B* **2006**, *110* (34), 16992–17000.

consistent with the higher reactivity of the NR tips,[51] and therefore coating these regions with ZnS helps to reduce the release of Cd appreciably.

There are however some remarks to be made to the discussion above. First of all, the above toxicity parameters have been calculated based on the values of $[Cd]_{cell}$ which were actually estimated on living cells, not on killed cells (as this was the only type of reliable estimate of intracellular concentration that could be made), while a stricter definition of toxicity should be related to the intracellular concentration of species that are actually found in the killed cells. Another important remark lies in the very definition of toxicity. If this is related to the number of killed cells upon exposure to a standard total concentration of Cd in the environment (i.e., 50 μM in the cases under discussion here), then the QDs are clearly more cytotoxic than the NR_S, since such total concentration of Cd corresponds to many more QDs than NRs, and we found in fact that proportionally more QDs particles are uptaken by the cells than NRs, which results in a higher toxicity. If on the other hand we consider our "normalized ξ-related intracellular toxicity" parameter, we find a higher toxicity of the double shell NRs sample with respect to the QD sample. In our opinion, this is in any case well compensated by the much higher brightness of the NRs, as discussed in the paragraph that follows.

To prove the potential exploitation of the double shell NRs as cell imaging tools, we acquired confocal images of HeLa cells stained with a solution of double shell NRs (at 50 μM Cd concentration) for 24 h. Under the same excitations and detection conditions, images of cells incubated either with core/shell NRs, double shell NRs or CdSe/ZnS QDs were acquired (at the same Cd concentration of 50 μM, see Figure 9). In Figure 9a, 8b, and 8c typical fluorescent signals are displayed, while in Figure 9d, 8e and 8f the corresponding bright field images are shown. From a qualitative point of view, it could be observed that the intensity of the fluorescent signal in the samples treated with the double shell sample is higher than in the other two cases. This could be considered as a preliminary indication of the higher brightness of the double shell NR sample. Since the nanoparticles were aspecifically up-taken, the fluorescent signal was distributed inside the cytoplasm, as generally observed in previous reports by other groups.[52,53] It should be evidenced that no sign of morphological damage of the cells was detectable and, for the case of double shell NRs, we observed cells in the mitosis phase (see for instance Figure 9c). A more quantitative assessment was possible by comparing the fluorescent signals from different samples of cell suspensions, each containing the same number of cells but doped with a different nanocrystal sample. The highest intensity of the PL signals was recorded indeed from the suspension of cells that had internalized the double shell NRs (Figure 9g). The higher signal recorded in the NRs compensates also for the lower number of rods in the cells as compared to the QDs.

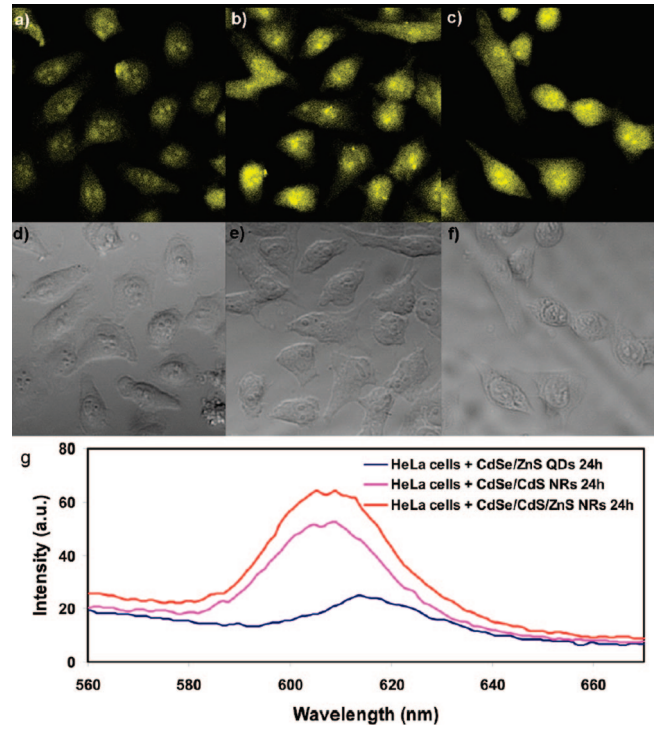

Figure 9. Confocal images of HeLa cells incubated with the CdSe/ZnS QD sample (a and d), with the CdSe/CdS core/shell NR sample (b and e) and with the CdSe/CdS/ZnS double shell NR sample (c and f) for 24 h at the same Cd concentration $[Cd]_{sol} = 50$ μM. Images a-c are acquired using a 488 excitation laser and a 605 $\pm$ 15 nm filter; d-f are bright field images. (g) Fluorescence spectra from different samples of cell suspensions, each containing the same number of cells but doped with a different type of nanocrystals (CdSe/ZnS QDs, core/shell NRs and double shell NRs). HeLa cells had been incubated with the nanocrystal solutions for 24 h at the same "total" Cd concentration (50 μM). The PL intensities were normalized to the number of cells.

4. Conclusions

We have reported the synthesis of CdSe/CdS/ZnS double shell NRs. The thin ZnS shell grown over the CdSe/CdS NRs leads to photoluminescence quantum efficiencies up to 75%. Time-resolved data corroborated the increase of free charge carriers due the presence of the ZnS shell, which reduced trapping and enhanced radiative recombination for higher quantum efficiency. The MTT cell viability assays, carried out by exposing cells to nanocrystal solutions at the same total concentration of Cd, indicated that covering the core/shell CdSe/CdS nanorods with a ZnS shell reduced their cell toxicity by 20%, and that both NR samples were less toxic than the QDs sample. Based on an "intracellular" toxicity parameter, defined by us as the number of killed cells divided by the intracellular total surface to volume ratio of nanoparticles, the double shell NRs were again less toxic than their parent CdSe/CdS NRs but both NR samples were more toxic than the CdSe/ZnS QDs. Such higher "intracellular toxicity" is however well compensated by the brighter intracellular PL signal recorded from cells doped with the double shell NRs than from those doped with QDs or with core/shell NRs. As a final remark, it is clear that the preparation of such double shell nanocrystals is more time and material consuming than for the starting core/shell nanorods, but in our opinion this is justified by the actual reduction of toxicity by 20%. Also, the sequential growth of the two shells can be made in principle in a one-pot approach, which should contribute to reduce the time and material (i.e., solvents/surfactants) effort required for their synthesis.

Acknowledgment. We thank Angela Fiore for helpful discussions. The Italian Ministry of Research (under contract number RBIN048TSE) is acknowledged.

(51) Carbone, L.; Kudera, S.; Giannini, C.; Ciccarella, G.; Cingolani, R.; Cozzoli, P. D.; Manna, L. *J. Mater. Chem.* **2006**, *16* (40), 3952–3956.
(52) Jaiswal, J. K.; Mattoussi, H.; Mauro, J. M.; Simon, S. M. *Nature Biotecnol.* **2003**, *21* (1), 47–51.
(53) Parak, W. J.; Pellegrino, T.; Plank, C. *Nanotechnology* **2005**, *16* (2), R9–R25.

Supporting Information Available: Details on the synthesis of the CdSe and CdSe/ZnS QDs and CdSe/CdS NRs. EELS imaging and sulfur mapping of ZnS QDs and CdSe/CdS/ZnS NRs. Surface functionalization of nanocrystals. Determination of nanocrystal concentration and the intracellular nanocrystals uptake. Additional details on the determination of PL QY of the various samples. Graph of integrated fluorescence intensity vs optical density of different samples in organic and aqueous solvents. Details on the preparation and characterization of water soluble nanocrystals. TEM images of the water soluble nanocrystals. UV−vis and PL spectra of the PEG functionalized nanocrystals. Gel electrophoretic characterization of the polymer-coated and PEG functionalized nanocrystal samples. DLS measurements on polymer-coated and PEG functionalized nanocrystal samples. Complete ref 22. This material is available free of charge via the Internet at http://pubs.acs.org.

JA808369E